Korean J. Chem. Eng., 40(9), 2165-2173 (2023)
DOI: 10.1007/s11814-023-1510-3

pISSN: 0256-1115
eISSN: 1975-7220

Electrochemical property based on the structural control of pitch-based carbon anode

Jin Ung Hwang*,, Ji Sun Im*,***,†, and Jong Dae Lee**,†**

*C1 Gas & Carbon Convergent Research Center, Korea Research Institute of Chemical Technology, 141 Gajeong-ro, Yuseong-gu, Daejeon 34114, Korea
**Department of Chemical Engineering, Chungbuk National University, 1 Chungdae-ro, Seowon-gu, Cheongju, Chungbuk 28644, Korea
***Advanced Materials and Chemical Engineering, University of Science and Technology (UST), 217, Gajeong-ro, Yuseong-gu, Daejeon 34113, Korea
(*Received 2 March 2023 • Revised 15 May 2023 • Accepted 9 June 2023*)

Abstract−The charge/discharge characteristics of a carbon anode were studied in a lithium ion battery system based on the effects of a graphite structure developed by heat energy. A carbon precursor (pitch) was synthesized from pyrolysis of fuel oil, after which a carbonization/graphitization treatment at 1,000-2,400 °C was carried out on the carbon anode. The lithium storage mechanism of carbonized materials treated under 1,300 °C was noted not by the space between the graphite layers but the cavity in the carbon materials. This indicates higher capacity and high speed charge-discharge performance capabilities than graphite. For graphitized materials treated at 2,400 °C, lithium ions are mainly inserted between the layers of the graphite, forming an interlayer structure. Based on the suggested mechanisms, it is noted that the charge/discharge of lithium ions can be controlled based on control of the graphite structure.

Keywords: Pitch, Carbon, Graphite, Anode, Lithium Ion Battery

INTRODUCTION

Since the commercialization of lithium ion batteries by Sony in 1991, lithium ion batteries have been widely used in small electronic devices and in portable devices. To overcome the limitations of hybrid electronic vehicles (HEV), electronic vehicles (EV) and electronic storage systems (ESS), it is necessary to improve the electrochemical performance of these batteries, such as their energy density, capacity and cycle retention performance. Lithium ion batteries are composed of a cathode, an anode, an electrolyte, and materials which separate these components. Carbon materials are most widely used for the anode. These carbon structures are composed of hexagonal and sp^2 structures, facilitating superior thermal conductivity compared to that in other metals. These structures can also be used as exothermal materials and as sensor materials [1,2].

As a precursor for carbon materials, pitch is produced by subjecting pyrolysis fuel oil (PFO) and coal tar to a heat treatment at temperatures of 200 to 500 °C for one to three hours. PFO-based pitch produced by the petroleum refining process has been studied as a carbon precursor given its low cost and low impurity content, its high carbon content, and its aromatic structure [3,4]. By controlling the temperature and time during the pitch-producing process, properties such as the mesophase content, softening point (S.P.) and quinoline insoluble (Q.I.) contents can be controlled. These factors affect temperature-dependent properties, such as the degree of graphitization and the electrical conductivity of the manufactured carbon materials. Kim et al. reformed PFO to produce pitch and analyzed the properties associated with changes in certain conditions, such as temperature and time. The electrochemical properties were also evaluated [5-8].

During the manufacturing process of carbon materials, the structure of the material depends on the manufacturing temperature. In lithium ion batteries, the lithium ion storage mechanism changes according to the structure of the carbon material. The characteristics of an amorphous structure arise when the manufacturing temperature of the carbon materials is in the range of 1,000-1,200 °C. Amorphous carbon consists of small hexagonal networks and exhibits a disordered structure that is poorly developed along the c-axis [9-11]. Thereby, there are many cavities and defects on the surface. Lithium ions are stored in the cavity and are transmitted to the inside by defects. When the manufacturing temperature of the carbon materials reaches 2,000 °C or higher, graphene forms a layered structure stacked many times with each layer connected by van der Waals force. These layered structures exchange electrons from the graphite surface through reactions with lithium ions in the organic electrolyte to provide a path by which lithium ions are stored. Lithium ions entering inside by the path accumulate between the graphite layers to form a lithium layer [12-14].

When one lithium layer is formed in the first reaction, during which lithium ions are inserted into the graphite negative electrode material, lithium ions are not inserted in the adjacent graphite layer. This produces a periodic arrangement of a layer of lithium ions and an empty graphite layer. Subsequently, as the number of lithium ions entering the interior increases, the lithium ion layer and the graphite layer become alternately arranged. As the amount of lithium increases, the potential of the graphite resembles that of lithium, and

†To whom correspondence should be addressed.
E-mail: jsim@krict.re.kr, jdlee@chungbuk.ac.kr

when the lithium capacity is reached (LiC_6), a volume change of 10% with a graphite structural change (ABAB→AAAA) occurs [15]. For this reason, research on lithium storage mechanisms and control of the carbon material structure depending on the manufacturing temperature of the carbon material is important for the further development of lithium ion batteries [16].

Many researchers have discussed the structural and electrochemical characteristics based on the manufacturing temperature using meso-carbon micro-beads (MCMB) and commercial graphite, and have presented charging/discharging mechanisms accompanying these characteristics. Other groups have studied the storage of lithium ions according to the charge/discharge potential of the carbon anode and according to structural changes of the anode material [17,18]. However, studies on structural changes at high C-rate according to the structural properties of carbon materials are still insufficient.

In this paper, we synthesized anode material at different manufacturing temperatures using low-cost petroleum residual oil. The charge/discharge mechanism according to the structure of the manufactured carbon material and the structural changes during high-speed charging and discharging were investigated in an experiment involving the use of ex-situ X-ray diffraction (ex-situ XRD). Carbon materials were prepared at various temperatures ranging from 1,000 to 2,400 °C, and the relationship between the bulk structure and electrochemical performance was studied. In addition, ex-situ XRD was used to investigate the structural change of carbon anode based on C-rate change. Also, this paper focuses on analyzing the electrochemical performance at a high C-rate. For this reason, a lower loading level than what is generally used was applied. In general, the thicker electrodes increased electrode resistance. While higher electrode thickness enhances experimental reliability, we encountered difficulties in obtaining the desired results. Therefore, in this paper, experiments at a high C-rate were necessary and the low current densities were accepted.

EXPERIMENTAL

1. Experimental Materials

We investigated the characteristics of the carbon material according to the manufacturing temperature and investigated the electrochemical properties by preparing an anode material using PFO as a raw material in order to analyze the rapid charging/discharging behavior according to the structural characteristics.

The carbon precursor used was produced using a pitch obtained by reacting petroleum byproducts generated in a domestic refinery in a 5 L batch-type autoclave under atmospheric conditions with a N_2 flow at a reforming temperature of 440 °C for 1 hour. The prepared PFO-based pitch was carbonized or graphitized at 1,000 to 2,400 °C (The temperature range of 1,000 to 1,700 °C is named carbonization process, and temperature of 2,100 and 2,400 °C is named graphitization process) to prepare a carbon material at each temperature tested. During the carbonization step, the PFO-based pitch was prepared at different synthesis temperatures ranging from 1,000 to 1,700 °C for one hour under atmospheric conditions with a N_2 flow of 100 cc/min and a heating rate of 5 °C/min. When using the graphitization process (2,100, 2,400 °C) directly with the pitch, the low-molecular-weight component of the pitch was volatilized, possibly leading to internal pollution inside the reactor, and carbonization was carried out at 1,000 °C under a nitrogen atmosphere for one hour. The graphitization process involved a pretreatment at 1,500 °C (10 °C/min, 2.5 hours, He atmosphere) and then proceeded at 2,100, 2,400 °C (15 °C/min for 1 hour, He atmosphere). Each sample was carbonized or graphitized, and the grain size was adjusted to 25 μm or less using a dry ball-mill, for eventual use as an anode material. These anode materials are called 4401P-X (X= 1,000-2,400).

2. Electrode Preparation, Cell Preparation and Physical/Electrochemical Characterization

To confirm the electrochemical characteristics of the carbon materials produced, Li metal was used as a counter electrode, and coin-type half cells were manufactured. The electrodes were prepared using a composition of 90 wt% of carbon active materials, 6 wt% of styrene-butadiene rubber (SBR, MTI korea), and 4 wt% of carboxymethyl cellulose (CMC, MTI Korea), while dendritic cupper foil (Wellcos Co., Republic of Korea) was utilized as the current collector for the negative electrode. First, the CMC and SBR were dissolved in deionized water, resulting in 1.5 wt% and 50 wt% solutions. After this step, the active materials and the binder were mixed according to the weight ratio, and the slurry was prepared by mixing at 2,000 rpm for 30 seconds and at 2,200 rpm for 30 seconds using a Thinky mixer (ARE-310, Thinky Co., Japan). The electrode slurry was cast on a Cu current collector (18 μm thick) by a doctor blade technique, resulting in electrodes. The electrodes were initially dried for 12 h at room temperature and afterwards dried under reduced pressure of at least 10 mbar for 12 h at 120 °C. The electrodes were manufactured by rolling a completely dried electrode and adjusting the electrode density to 1.2 to 1.5 g/cm^3. In addition, lower loading levels (4.0 to 5.0 mg/cm^3) were used for high-C-rate experiments than generally used. They were then cut with 12 mm diameters to produce coin-type electrodes. Lithium foil was used as the counter electrode in the coin-type cells for the electrochemical test. The electrolyte was a 1 M $LiPF_6$ solution in a mixture of ethylene carbonate (EC) and diethyl carbonate (DEC) (1/1 vol%. Wellcos Co., Republic of Korea).

To investigate the structural characteristics of the manufactured carbon material and its structural characteristics under the insertion/desorption conditions of lithium ions used X-ray diffraction (XRD, Rigaku D/Max 2,200 V, Bruker: CuKα radiation). The samples were scanned in a 2θ range of 2 to 80° with a step size of 0.02°. To observe the structural features under high-speed charge/discharge conditions, we disassembled batteries after complete charging and discharging at each C-rate (0.1 C, 20 C, re-0.1 C). The 1 C-rate was set based on the general capacity of graphite (300 mAh/g).

This was done in a glove box maintained in an Ar atmosphere to prevent side reactions due to air contact with the electrolyte and lithium during the manufacturing of the sample used in the analysis. In addition, to evaluate the electrochemical characteristics of the fabricated half-cells, charge/discharge and C-rate characteristic tests were carried out using a WBCS 3000 Battery Cycler (Won A Tech, Republic of Korea). The charge-discharge and C-rate tests were carried out in the constant current-constant voltage (CC-CV) mode, the cut-off voltage was set to range from 0.01 to 2.0 V, and

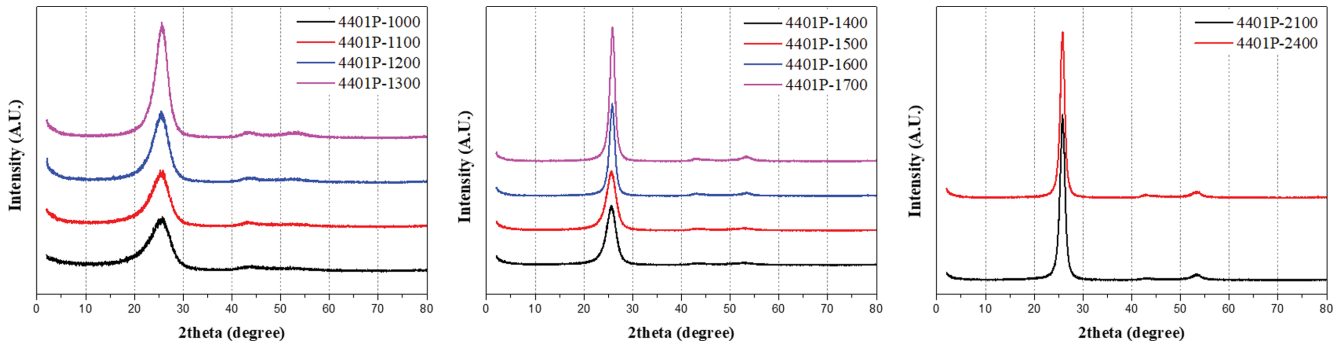

Fig. 1. X-ray diffraction patterns of the PFO-based carbon material with the heat-treatment temperature.

the speed characteristics were tested at the different C-rates of 0.1 C, 0.5 C, 1 C, 2 C, 5 C, 10 C, 20 C, and re-0.1 C. Cyclic voltammetry (CV) was measured by a ZIVE SP2 electrochemical test system (Won A Tech, Republic of Korea) at a scan rate of 0.1 mV/s and cut-off voltage was set to range from 0.01 to 3.0 V.

High-resolution transmission electron microscopy (HR-TEM, FEI Tecnai G2 20 TEM, Hillsboro, USA) and fast Fourier transform (FFT) were used to analyze the morphology and crystalline structure of carbon materials.

X-ray photoelectron spectroscopy (XPS, KRATOS AXIS NOVA, Bruker: Al Kα radiation) spectra were taken with Al Kα radiation (1,486.6 eV). The C 1s peak of carbon was used as a reference for the chemical shift determination, assuming that its binding energy was 284.5 eV.

The carbon materials were heated in vacuum condition at 200 °C for 8 h to remove water and certain impurities that had been adsorbed before analysis; this was the same preparation method used in the Brunauer-Emmett-Teller (BET) analysis because we assumed that the same conditions must be reached before performing analysis. The pore structures of the samples were confirmed by N2 adsorption analysis at 87.34 K using an ASAP2020 (Micromeritics, USA). The specific surface areas of the samples were obtained by BET equations.

RESULTS AND DISCUSSION

1. Correlation Between the Structural Characteristics and Electrochemical Characteristics Depending on the Manufacturing Temperature

X-ray diffraction (XRD) studies were conducted to calculate the development of the interlayer spacing (d(002)) and the thickness of stacks (L_c) of carbon, as shown in Figs. 1 and 2. The Bragg equation was used to determine the interlayer spacing and thickness of the stacks ([19-22]: $d(002)=\lambda/2\sin\theta_c$, $L_c=0.89\lambda/\beta\cos\theta_c$, where λ is the wavelength of CuKα (1.54 Å). The angle of the peak d(002) and the full width at half maximum (FWHM) were sourced from the XRD pattern.

In the graph, it was confirmed that the intensity of the XRD peak increased as the processing temperature of the carbon material increased, with a gradual shift of the d(002) reflection to the high diffraction angle side. As reported by Fromm et al., in general, the peak corresponding to d(002) shifts to the right as the carbonization temperature increases, and this phenomenon indicates increase of stacking of carbon layer and decrease of the interlayer spacing of the (002) plane by homogeneous graphitization [18].

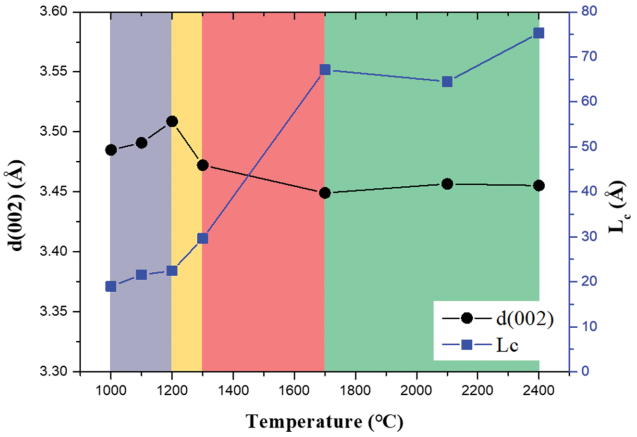

Fig. 2. Relationship between d(002) and L_c with the heat-treatment temperature.

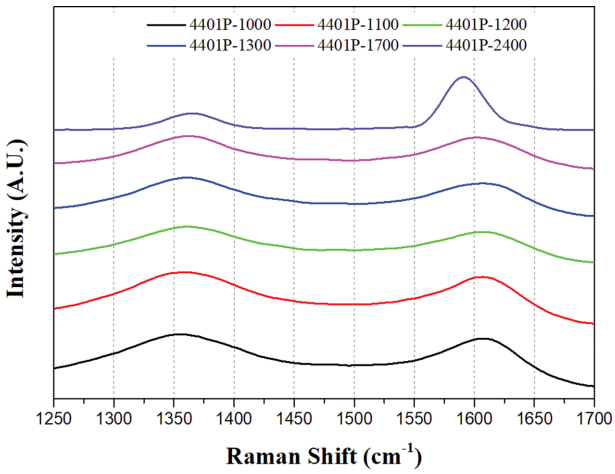

Fig. 3. Raman spectra of PFO based anode materials with different heat-treatment temperature.

The investigation of graphite structure was discussed based on Raman spectra result in Fig. 3 and Fig. 4. Fig. 3 shows the Raman spectra of all carbonaceous materials treated at various tempera-

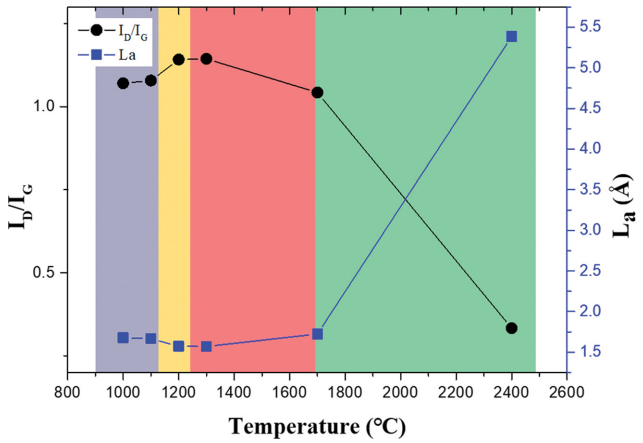

Fig. 4. Relationship between I_D/I_G, L_a and heat-treatment temperature.

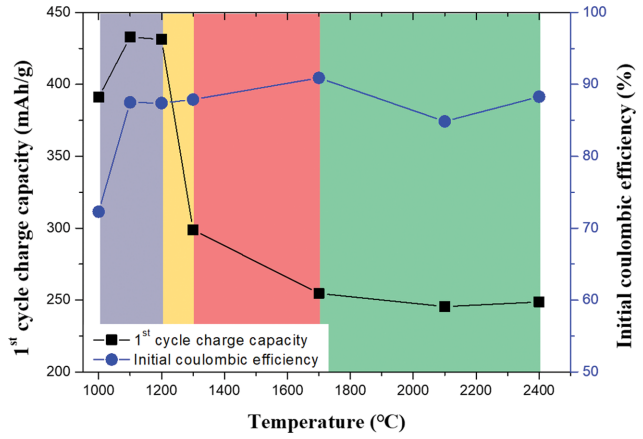

Fig. 5. First charge capacity and initial coulombic efficiency of PFO-based carbon anode materials.

ture. The ratio of D-band (1,350 cm^{-1}) and G-band (1,580 cm^{-1}) intensity (I_D/I_G) is useful to characterize the graphite (hexagonal) structural changes in carbonaceous materials. The overlapping area of two peaks was attenuated at higher treatment temperature, and it is noted that graphite structure and domain size is developed. The relation between I_D/I_G and treatment temperature is shown in Fig. 4. The I_D/I_G ratios decreased dramatically over 4401P-1700, indicating a higher degree of graphitization and smaller void spaces by defects. This development of graphite structure is contributed by X-axis structure growth as shown by increased La.

Transmission electron microscopy (TEM) and fast Fourier transform (FFT) image of Fig. S1 shows the crystal structure of carbon materials. The amorphous carbon structure is observed in Fig. S1(a) and (b). On the other hand, the developed carbon structure was confirmed in FFT image of Fig. S1(c). The FFT spectra of 4401P-2400 are distributed concentrically. The symmetric property of the power spectrums (FFT spectra) indicates the isotropic structure [31].

Fig. 5 presents an overview of the development of the initial charge capacity and the initial Coulombic efficiency at the different carbonization/graphitization temperatures. In the temperature

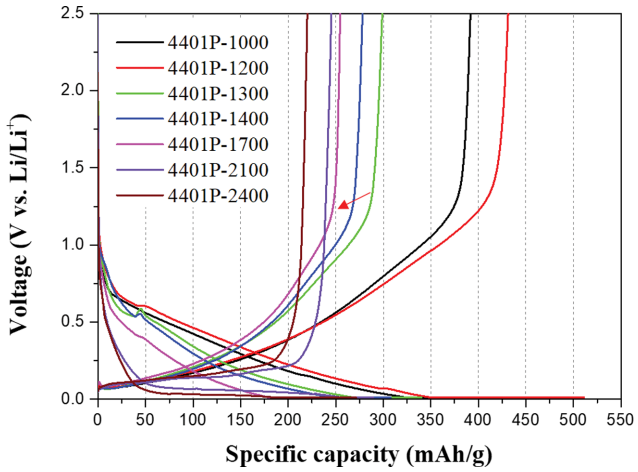

Fig. 6. First charge discharge profile of PFO-based carbon anode materials.

range of 1,000 to 1,200 °C, the charge capacity increased with the increase heat-treatment temperature. There is no definite clarification as to the phenomenon of the initial capacity increase at the low carbonization temperature. But, according to results by Mabuchi, carbon material treated at a relatively low temperature determines the properties of soft carbon. The lithium storage mechanism of soft carbon does not depend on lithium ion storage between carbon layers. Instead, a capacity higher than the theoretical capacity of graphite (~372 mAh/g) is measured by the mechanism by which the lithium ions in the cavities in the material are preserved [17].

The initial capacity of 1,200 to 1,300 °C shows a very sharp decrease. As compared with the previous temperature section, d(002) decreases and the L_c value shows a tendency to increase. In this temperature range, it has been reported that as the heat treatment progresses in the carbon material, the cavity structure present in the carbon material decreases [13]. This has been interpreted as stemming from the decrease in the initial capacity generated when lithium is stored in the cavity.

The initial capacity of the carbon material produced at a temperature in the range of 1,300 to 1,700 °C decreases. However, there is no large initial capacity reduction matching that in the previous temperature range. The changes in d(002) and L_c are similar to the change in the initial capacity. This is interpreted as being caused by a decrease in the lithium ion capacity of amorphous carbon due to the development of a carbon structure, unlike the decrease of the cavity structure which existed in the previous temperature range. This is indicated by the red arrow in Fig. 6.

The initial capacity and initial Coulombic efficiency at 1,700 to 2,400 °C do not change significantly. In the carbon structure in this temperature range, the rate of increase in the L_c value decreases due to the ensuing rearrangement. According to Mabuchi et al., the initial capacity of the carbon material is known to be greatly affected by the structural development on the c axis. However, the initial efficiency appeared to be somewhat reduced due to the development of a graphite structure accompanying the rise in the temperature and the increased number of side reactions at the edge part [17].

Fig. 6 shows a graph of the initial charge-discharge properties of the samples, devised to compare lithium insertion types according to the structure of the carbon material used. The prepared samples show two types of charge-discharge curve shapes. The first type is a gradient charge-discharge curve, which is observed with an amorphous carbon anode material. This type of charge-discharge curve shows the hysteresis phenomenon, in which the lithium desorption potential appears higher than the lithium insertion potential. This is observed in the temperature range of 1,000 to 1,700 °C. Moreover, as the manufacturing temperature increases, the hysteresis phenomenon decreases [23]. The above phenomenon is related to the carbon and oxygen contents of carbon material. XPS survey-scan spectrum of 4401P-1300, 4401P-2400 sample in the binding energy range of 0-1,000 eV indicated the presence of carbon and oxygen as shown in Fig. S2. Carbonized material at lower temperatures has more oxygen content (1.6→6.3%). Such an increase in oxygen functional groups can enhance the reaction of forming the SEI layer such as Li_2CO_3 [18].

The second type is a charge-discharge curve in which the staging phenomenon and the plateau section observed with the insertion of lithium into a carbon anode material with a graphite structure are observed. In this type of discharge curve, the staging phenomenon is observed at 0.2 V vs. Li/Li^+, which arises when lithium ions are inserted between the graphite layers. As a result, it can be confirmed indirectly that the layer structure of graphite has developed. The difference in the shape of the initial charge-discharge graph depending on the manufacturing temperature of the carbon anode material is most affected by the difference in the lithium ion insertion mechanism depending on the structure of the carbon material. The insertion of lithium in soft carbon with an amorphous structure will be done through the defects and cavities given the disordered structure. Therefore, the potential plateau section indicated by 1 V vs. Li/Li^+ observed during lithium insertion into a carbon structure in which the layer structure is generally formed is eliminated. Therefore, the inclined lithium ion insertion curve arises [24].

An additional analysis was carried out by confirming that the abrupt structure and electrochemical properties change at 4401P-1300 among the results of Fig. 2 and Fig. 5. Fig. 7 shows the charge-discharge curves of the first and second cycles for the sample treated at 1,300 °C. The initial discharge capacity of the material was measured at 323.2 mAh/g and the initial charging and discharging efficiency was measured at 88.9%. Note that when comparing the charging/discharging graphs, the lithium desorption graph resembles the graph of another amorphous carbon material, but other lithium insertion behavior is shown in the lithium insertion graph. There is a change in the differential capacity value in the vicinity of 0.6 V vs. Li/Li^+ in the first cycle. This is a phenomenon by which lithium ions stored in the cavity on the surface of the material in the first cycle assist in the formation reaction of the SEI (solid electrolyte interface) layer with the electrolytic solution, resulting in the phenomenon by which the potential rises. A broad peak is shown from the second charge-discharge curve, indicating stable graph formation.

CV analysis was carried out to investigate the behavior of lithium ion during charge-discharge process. The CV analysis for 4401P-1000~4401P-2400 samples was performed at a scan rate of 0.1 mV/s in the voltage range of 0.01 to 3.0 V, and the results are shown Fig. 8. A similar trend of CV curve can be observed between (a)-(d). In general, the broad peak was observed at 0.5-0.8 V vs. Li/Li^+ (peak 1), which is a reduction peak and related to the formation of SEI layer on the surface [25]. Specifically, 4401P-1000, which has many cavities on the surface, showed the broad peak at first cycle. This reduction peak was attenuated by higher treatment temperature. It is noted that the cavity should be controlled for stable charge-discharge process. Eventually, a different type CV curve was observed in 4401P-2400. The broad reduction peak was shifted to 1.0 V vs. Li/Li^+ (peak 2). It is noted that the lithium ion storage by pore (or defect) was carried out at higher applied voltage than SEI layer formation, relatively. Also, the sharp oxidation peak located at 0.01 V vs. Li/Li^+ (peak 3) is related to the intercalation of lithium ion for the graphitic structure. This peak became shaper at higher treatment temperature. The oxidation peak (peak 4) was observed more clearly with a higher cycle which is related to de-intercalation of lithium ion. Most importantly, the CV curves (except 1st cycle) were almost overlapped, which means an excellent electrochemical reversibility [26].

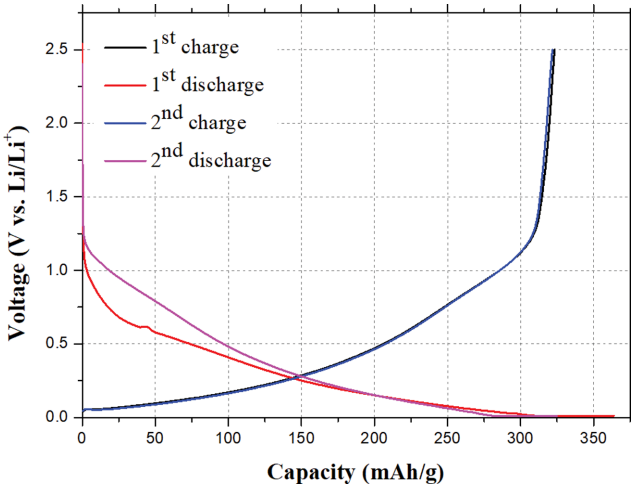

Fig. 7. Charge-discharge profile of PFO-based carbon anode materials heat-treated at 4401P-1300.

Experiments were carried out to analyze the changes in the properties of the C-rate and cycle retention depending on the production temperature of the carbon material. These results are shown in Fig. 9 and Fig. 10. In the cycle retention test, the charge-discharge was repeated for five cycles at 0.1 C to form a stable SEI layer, and the capacity was measured at 1 C for 100 cycle. The 20 C/0.1 C C-rate performance outcomes of the manufactured carbon material were as follows: 4401P-1000 at 78%, 4401P-1200 at 87%, 4401P-1400 at 79%, 4401P-1700 at 73% and 4401P-2400 at 60%. The maximum speed characteristic efficiency was found at 1,200 °C, after which it tended to be lower. And the cycle retention performance was also investigated as follows: 4401P-1,000 at 29%, 4401P-1200 at 73%, 4401P-1300 at 76%, 4401P-1700 at 76% and 4401P-2400 at 90%. It is noted that the capacity retention rate increased at higher treatment temperature.

This is considered to be due to the insertion/desorption mecha-

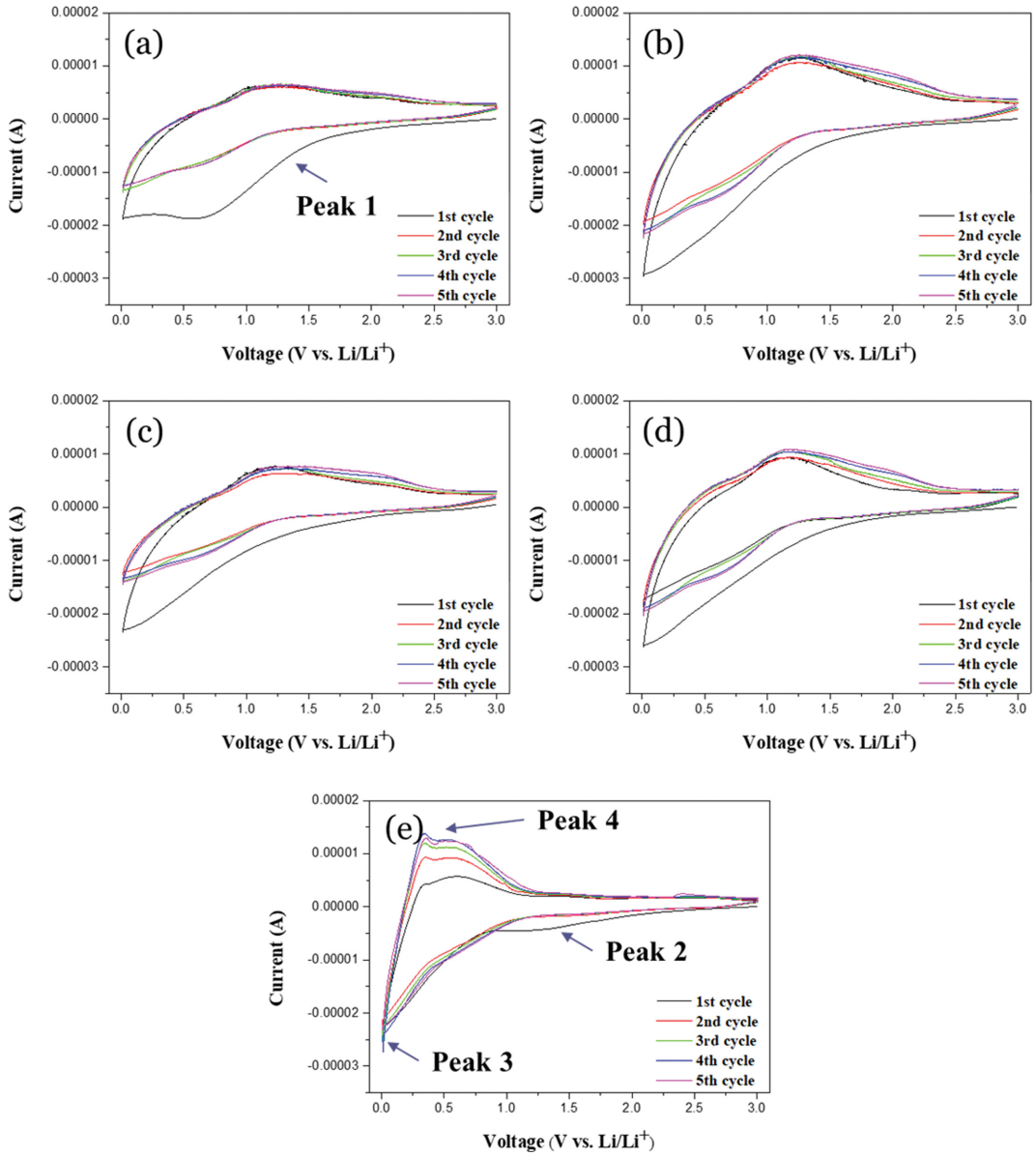

Fig. 8. Cyclic-voltammetry curve of PFO based carbon anode materials heat treated at (a) 4401P-1000, (b) 4401P-1200, (c) 4401P-1300, (d) 4401P-1300, (e) 4401P-2400.

nism of the lithium ions in the carbon material, depending on the manufacturing temperature. According to Kim et al., defects and cavities exist at the site where lithium ions are stored or on the path when lithium ions are inserted/deserted [27]. The above characteristics are consistent with Tokumitsu's and Kim's research results. According to that research, when the heat treatment temperature of MCMB increases, the cavity for lithium ion storage space decreases and the capacity decreases [28-30].

Therefore, when the structural characteristics of the carbon material are developed by a high manufacturing temperature, the stability of lithium ion preservation improves but the numbers of sites and paths decrease, the length of migration of the lithium ions increases, and the speed characteristics may deteriorate. Experiments were also conducted using ex-situ XRD to examine the structural changes due to lithium insertion/desertion and the charging/discharging rate depending on the structure of the carbon material.

2. Structure of the Manufactured Material and Structural Changes Due to the Charge-discharge Speed

Fig. 11 shows the ex-situ XRD patterns of 4401P-2400 under Li-ion intercalation/de-intercalation with different charging C-rates. Table 1 shows the calculated d(002) and L_c values. To observe the structural change due to the charging/discharging rate, an electrode coated with the carbon material was intercalated with lithium ions at a rate of 0.1 C, after which the coin-type cell was separated and washed with dimethyl carbonate (DMC) solvent. The electrode was washed and dried to prepare a sample, referred to as the 0.1 C Li^+ intercalation sample. Samples in which lithium ions were de-intercalated at a rate of 0.1 C after intercalation were prepared using the same method and termed 0.1 C Li^+ de-intercalation samples. In addition, 20 C intercalation/de-intercalation samples were man-

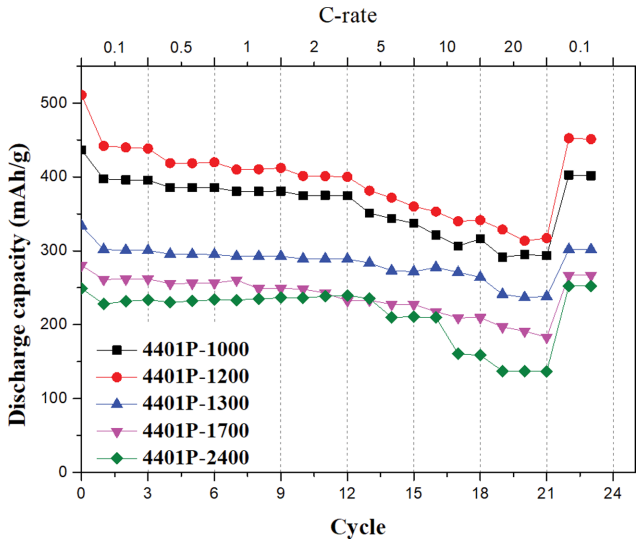

Fig. 9. Discharging capacities of PFO-based carbon anode materials at 4401P-1000~4401P-2400, when measured at different C-rates.

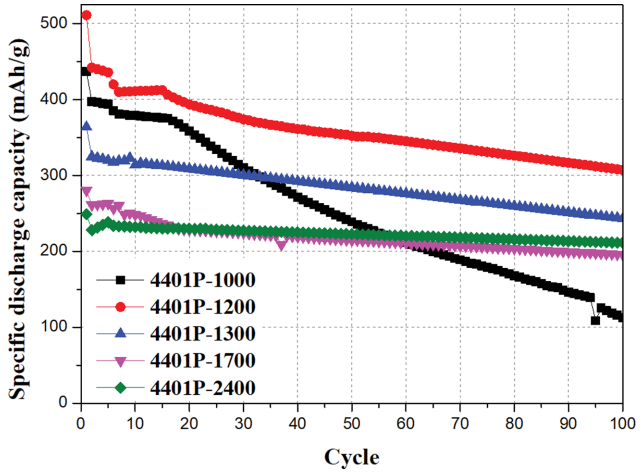

Fig. 10. Cycle retention test of PFO based carbon anode materials at 4401P-1000~4401P-2400.

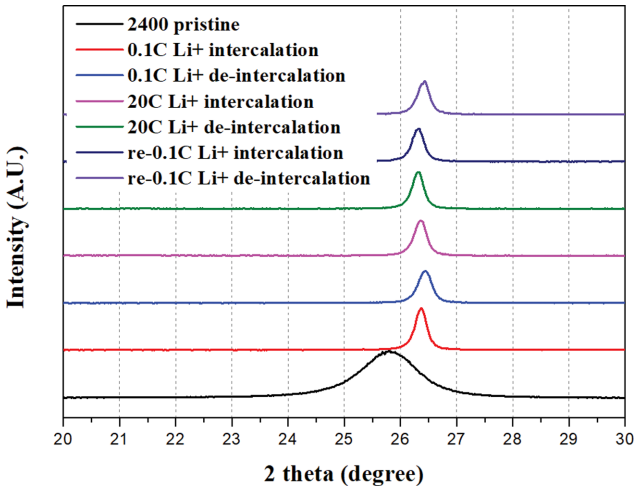

Fig. 11. Ex-situ XRD patterns of the PFO-based carbon material under Li-ion intercalation/de-intercalation with different charging C-rates (4401P-2400).

Table 1. Ex-situ XRD patterns of the PFO-based carbon material under Li-ion intercalation/de-intercalation when different charging C-rates (4401P-2400)

	(002) peak		L_c (Å)
	2-theta (deg.)	d (Å)	
2400 pristine	25.75	3.46	64.55
0.1 C Li^+ intercalation.	26.36	3.38	346.28
0.1 C Li^+ de-intercalation.	26.43	3.37	286.96
20 C Li^+ intercalation.	26.36	3.38	315.05
20 C Li^+ de-intercalation.	26.30	3.39	343.28
re-0.1C Li^+ intercalation.	26.30	3.39	341.82
re-0.1C Li^+ de-intercalation.	26.41	3.37	332.01

ufactured by increasing the current in the order of 0.1, 0.5, 1, 2, 5, 10, and 20 C for stable experiments under high-speed charging and discharging. In addition, when the experiment was conducted again at a low charge/discharge speed, in order to observe the changes in and recovery of the carbon structure, the sample with intercalation/de-intercalation lithium ions at a rate of 0.1 C after 20 C was named re-0.1 C in the sample preparation process.

When inserting lithium ions at a 0.1 C-rate, the existing XRD peak moved to a low scattering angle. In addition, when lithium ions were desorbed to 1.5 V vs. Li/Li^+ at the same current density, the phenomenon by which the peak moves relatively upward was shown. Despite the de-intercalation of lithium ions in the 20 C de-intercalation sample, the position of the peak does not change significantly. This appears to be a phenomenon due to the mobility of lithium ions corresponding to the characteristics of the sample at a high current density at the time of lithium de-intercalation. In general, carbon materials manufactured at 3,000 °C or higher develop a graphite structure via d(002), d(004) and d(100). The carbon material produced in this paper has low graphitization due to its low heat-treatment temperature. It is conceivable that it shows low electric conductivity and low lithium ion mobility accordingly. Such characteristics limit the movement of lithium ions at a high current density. Therefore, lithium de-intercalation was not performed, and it was considered that the structure does not change. In addition, the crystallinity of the carbon material increases when lithium ions undergo intercalation/de-intercalation. This most likely occurs because the disordered structure of the carbon surface changes the stacking structure by the shearing force induced by the insertion/desertion of lithium ions. The disordered structure of the surface part is restored to the layered structure [31].

Fig. 12 shows ex-situ XRD patterns of 4401P-1300 under Li-ion

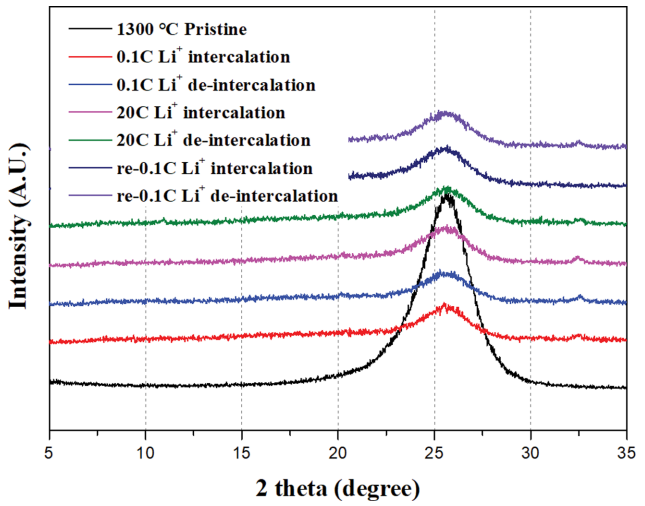

Fig. 12. Ex-situ XRD patterns of the PFO-based carbon material under Li-ion intercalation/de-intercalation with different charging C-rates (4401P-1300).

Table 2. Ex-situ XRD patterns of the PFO-based carbon material under Li-ion intercalation/de-intercalation with different charging C-rates (4401P-1300)

	(002) peak		L_c (Å)
	2-theta (deg.)	d (Å)	
1300 pristine	25.63	3.47	29.61
0.1 C Li^+ intercalation	25.50	3.49	30.27
0.1 C Li^+ de-intercalation	25.57	3.48	28.25
20 C Li^+ intercalation	25.68	3.47	35.80
20 C Li^+ de-intercalation	25.77	3.45	38.62
re-0.1C Li^+ intercalation	25.63	3.47	33.70
re-0.1C Li^+ de-intercalation	25.63	3.47	37.99

intercalation/de-intercalation with different charging C-rates. In general, low crystalline carbon is difficult to analyze peaks due to diffraction from a plurality of directions during XRD analysis. Table 2 shows the calculated d(002) and L_c values. The sample preparation method is identical to that in Fig. 7 and Table 1. A broad amorphous peak is observed compared to the carbon material manufactured at 4401P-2400. A peak at 25.63°, corresponding to the (002) peak, moved to 25.50° due to the insertion of lithium ions with the same tendency noted in the above experiment. Moreover, at the time of lithium ion desorption at the 0.1 C-rate, the peak shifted slightly at 25.57°. These behaviors are interpreted as differences depending on the structure of the carbon material used. Because the sample at 4401P-1300 does not depend on the intercalation of lithium ions and given that lithium ions are inserted into the cavity, this outcome shows the difference in the structural change accompanying the insertion and desorption of lithium, as described above. Additionally, the insertion and desorption behavior of lithium at 20 C-rate is similar to that at the 0.1 C-rate. However, it can be confirmed that the change in the structure when lithium ions rapidly undergo insertion/desertion incurs a relatively large change in the L_c value as compared to the insertion/desertion of low-speed lithium ions.

This phenomenon can be interpreted as being identical to the result of the electrochemical test performed above. The insertion of lithium ions into an amorphous carbon structure progresses via a mechanism stored in the cavity rather than through intercalation by staging between carbon layers at potentials of less than 0.2 V vs. Li/Li^+. This phenomenon is described by the charge-discharge profile, divided into two sections. The capacitance according to the potential is measured as shown in Table 3 based on 0.2 V vs. Li/Li^+, which is the potential at which lithium ions are staged inside the graphite layer. "A" represents the total discharge capacity, "B" represents the reference potential or less, and "C" represents a capacity higher than the reference potential. In the carbon material produced at 4401P-1300, a proportion of approximately 57% of the stored lithium ions is inserted between the graphite layers, and in the carbon material produced at 4401P-2400, a ratio of 91% is inserted between the graphite layers. Therefore, 42% and 9% of lithium ions can be interpreted as being stored in cavities or defects, but not via interlayer insertion.

To discuss the pore structure, the nitrogen adsorption-desorption isotherm of Fig. S3 is shown. The BET specific surface area of the 4401P-1300 and 4401P-2400 was 9.67 and 7.19 m^2/g, respectively. The specific surface area has a relevance to the initial capacity (lithium ion insertion). At this time, lithium ions are not inserted into the graphite layer, but lithium is stored in the pore of surface. In addition, isotherms of 4401P-2400 exhibit a hysteresis, indicating the presence of mesopore. And the pore structure of material can enhance the electrochemical performance such as a high rate performance. Therefore, the currently fabricated 4401P-2400 sample might show a high rate performance.

CONCLUSION

Pitch-based carbon materials were produced by carbonization/

Table 3. Discharge capacities of carbon materials with the heat-treatment temperature (First region: capacity under 0.2 V vs. Li/Li^+, second region: capacity over 0.2 V vs. Li/Li^+)

Heat treatment temperature (°C)	Discharge capacity (mAh/g) - A	1st region capacity (mAh/g) - B	2nd region capacity (mAh/g) - C	C/A*100 (%)
4401P-1300	340.232	194.369	145.863	57.12837
4401P-2400	266.001	243.0422	22.9588	91.3689

graphitization in order to consider the charge-discharge characteristics of anode material based on the heat-treatment temperature of the carbon materials. The electrochemical characteristics were studied based on structural development and structural changes of prepared carbon anode. The structural change of P4401-1300 and P4401-2400 was investigated at various C-rate. P4401-1300 has an amorphous structure and cavities on the surface. And amorphous carbon structure was not changed under C-rate (0.1 and 20), because most lithium ions were conserved in pores and defects. On the other hand, P4401-2400 developed carbon structure. And carbon structure was changed on 0.1 C-rate. Lc expanded due to intercalation of lithium ion (286.96→346.28 Å). But carbon structure was not charged under high 20 C-rate condition. It is considered that low lithium mobility caused the low electrical conductivity.

ACKNOWLEDGEMENTS

This work was supported by the Korea Evaluation Institute of Industrial Technology (KEIT) through the Carbon Cluster Construction project [10083621, Development of Preparation Technology in Petroleum-Based Artificial Graphite Anode] and Technology Innovation Program [20006696, Development of isotropic graphite block for semiconductor process] funded by the Ministry of Trade, Industry & Energy (MOTIE, Korea).

SUPPORTING INFORMATION

Additional information as noted in the text. This information is available via the Internet at http://www.springer.com/chemistry/journal/11814.

REFERENCES

1. B. H. Kim, J. H. Kim, J. G. Kim, M. J. Bae, J. S. Im, C. W. Lee and S. Kim, *J. Ind. Eng. Chem.*, **41**, 1 (2016).
2. J. F. Peters, M. Baumann, B. Zimmermann, J. Braun and M. Weil, *Renew. Sust. Energy Rev.*, **67**, 491 (2017).
3. J. G. Kim, J. H. Kim, B. J. Song, C. W. Lee and J. S. Im, *J. Ind. Eng. Chem.*, **36**, 293 (2016).
4. J. G. Kim, J. H. Kim, B. J. Song, Y. P. Jeon, C. W. Lee, Y. S. Lee and J. S. Im, *Fuel*, **167**, 25 (2016).
5. B. H. Kim, J. H. Kim, J. G. Kim, J. S. Im, C. W. Lee and S. Kim, *J. Ind. Eng. Chem.*, **45**, 99 (2017).
6. J. G. Kim, F. Liu, C. W. Lee, Y. S. Lee and J. S. Im, *Solid State Sci.*, **34**, 38 (2014).
7. M. Pérez, M. Granda, R. Garcia, R. Santamaría, E. Romero and R. Menéndez, *J. Anal. Appl. Pyrolysis*, **63**, 223-239 (2002).
8. S. Huang, H. Guo, X. Li, Z. Wang, L. Gan, J. Wang and W. Xiao, *J. Solid State Electrochem.*, **17**(5), 1401 (2013).
9. S. Dong, P. Alvarez, N. Paterson, D. R. Dugwell and R. Kandiyoti, *Energy Fuels*, **23**(3), 1651 (2009).
10. J. C. Lascovich, R. Giorgi and S. Scaglione, *Appl. Surf. Sci.*, **47**(1), 17 (1991).
11. R. E. Franklin, *Proc. R. Soc. Lond. A*, **209**(1097), 196 (1951).
12. M. Winter, J. O. Besenhard, M. E. Spahr and P. Novak, *Adv. Mater.*, **10**(10), 725 (1998).
13. J. R. Dahn, T. Zheng, Y. Liu and J. S. Xue, *Science*, **270**(5236), 590 (1995).
14. J. Wang, J. L. Liu, Y. G. Wang, C. X. Wang and Y. Y. Xia, *Electrochim. Acta*, **74**, 1 (2012).
15. Z. Ogumi and M. Inaba, *Bull. Chem. Soc. Jpn.*, **71**(3), 521 (1998).
16. N. A. Kaskhedikar and J. Maier, *Adv. Mater.*, **21**(25-26), 2664 (2009).
17. A. Mabuchi, K. Tokumitsu, H. Fujimoto and T. Kasuh, *J. Electrochem. Soc.*, **142**(4), 1041 (1995).
18. O. Fromm, A. Heckmann, U. C. Rodehorst, J. Frerichs, D. Becker, M. Winter and T. Placke, *Carbon*, **128**, 147 (2018).
19. B. Manoj and A. G. Kunjomana, *Int. J. Electrochem. Sci.*, **7**(4), 3127 (2012).
20. N. S. Saenko, *Phys. Procedia*, **23**, 102 (2012).
21. M. D. Awitdrus, I. A. Talib, R. Omar, M. H. H. Jumali, E. Taer and M. M. Saman, *Sains Malaysiana*, **39**(1), 83 (2010).
22. C. N. Barnakov, G. P. Khokhlova, A. N. Popova, S. A. Sozinov and Z. R. Ismagilov, *Eurasian Chemico-Technological J.*, **17**(2), 87 (2015).
23. Y. J. Han, D. Chung, K. Nakabayashi, J. D. Chung, J. Miyawaki and S. H. Yoon, *Electrochim. Acta*, **213**, 432 (2016).
24. S. Flandrois and B. Simon, *Carbon*, **37**, 165 (1999).
25. B. Xing, C. Zhang, Y. Cao, G. Huang, Q. Liu, C. Zhang, Z. Chen, G. Yi, L. Chen and J. Yu, *Fuel Process. Technol.*, **172**, 162 (2018).
26. J. U. Hwang and J. D. Lee, *Korea Chem. Eng. Res.*, **55**(3), 307 (2017).
27. L. Ji, Z. Lin, M. Alcoutlabi and X. Zhang, *Energy Environ. Sci.*, **4**(8), 2682 (2011).
28. K. Tokumitsu, H. Fujimoto, A. Mabuchi and T. Kasuh, *Carbon*, **37**(10), 1599 (1999).
29. H. Kim, W. Choi, J. Yoon, J. H. Um, W. Lee, J. Kim, J. Cabana and W.-S. Yoon, *Chem. Rev.*, **120**(14), 6934 (2020).
30. C. W. Park and S. M. Oh, *J. Korean Electrochem. Soc.*, **2**(4), 221 (1999).
31. S. E. Lee, J. H. Kim, Y. S. Lee, B. C. Bai and J. S. Im, *Carbon Lett.*, **31**, 911 (2021).

Supporting Information

Electrochemical property based on the structural control of pitch-based carbon anode

Jin Ung Hwang[*,**], **Ji Sun Im**[*,***,†], **and Jong Dae Lee**[**,†]

*C1 Gas & Carbon Convergent Research Center, Korea Research Institute of Chemical Technology,
141 Gajeong-ro, Yuseong-gu, Daejeon 34114, Korea
**Department of Chemical Engineering, Chungbuk National University,
1 Chungdae-ro, Seowon-gu, Cheongju, Chungbuk 28644, Korea
***Advanced Materials and Chemical Engineering, University of Science and Technology (UST),
217, Gajeong-ro, Yuseong-gu, Daejeon 34113, Korea
(*Received 2 March 2023 • Revised 15 May 2023 • Accepted 9 June 2023*)

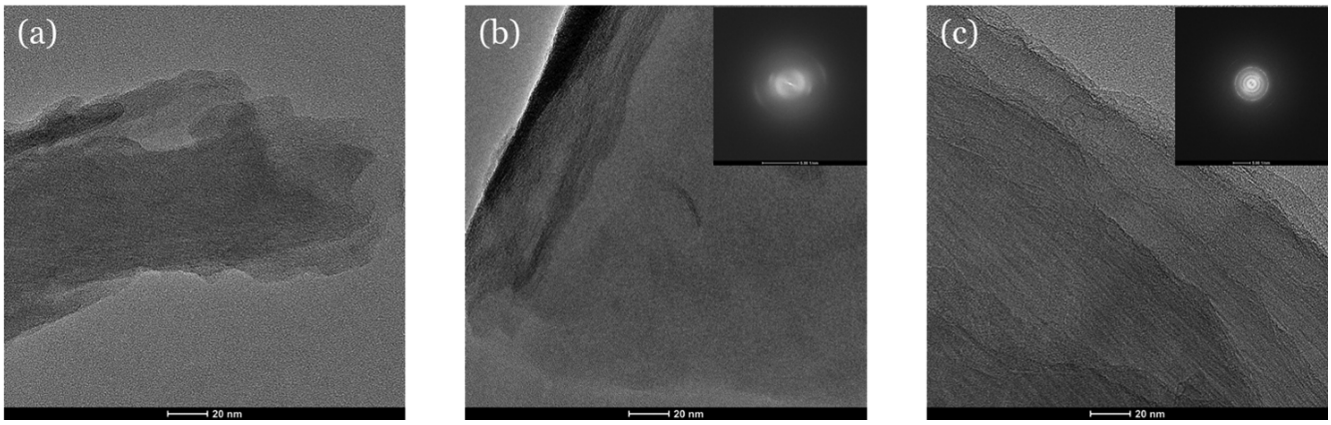

Fig. S1. HR-TEM and FFT images (right, inset) of pitch-based carbon material (a) P4401-1000, (b) P4401-1300, (c) P4401-2400.

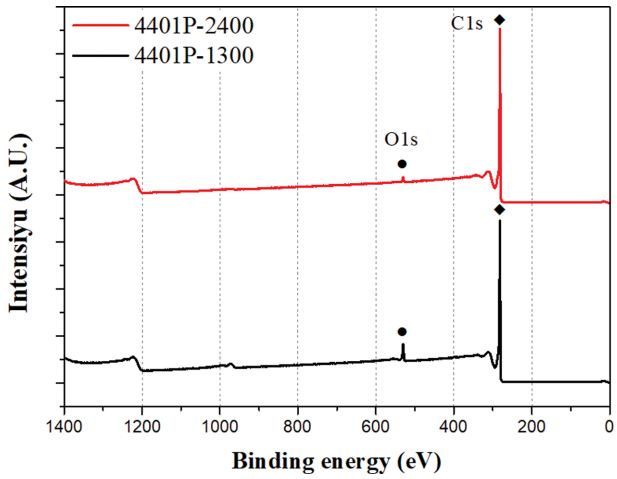

Fig. S2. XPS survey scan of pitch-based carbon material.

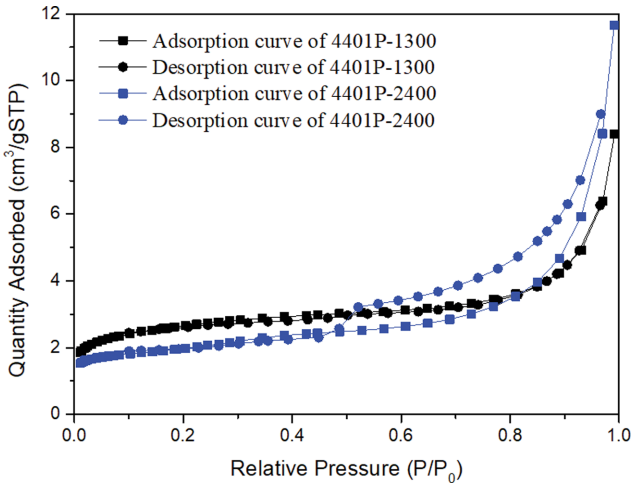

Fig. S3. Nitrogen adsorption-desorption isotherm of pitch-based carbon material.